ELSEVIER

International Journal of Solids and Structures 41 (2004) 2521–2537

INTERNATIONAL JOURNAL OF SOLIDS and STRUCTURES

www.elsevier.com/locate/ijsolstr

A numerical method for the exact elastic beam theory. Applications to homogeneous and composite beams

Rached El Fatmi, Hatem Zenzri *

Département de Génie Civil, Ecole Nationale d'Ingénieurs de Tunis, B.P. 37, 1002 Le Belvédère, Tunis, Tunisia

Received 4 June 2003; received in revised form 18 November 2003

Abstract

The purpose of this paper is to simplify the numerical implementation of the exact elastic beam theory in order to allow an inexpensive and large use of it. A finite element method is proposed for the computation of the beam operators involved in this theory. These operators are required for the calculation of the one-dimensional structural beam behavior and the three-dimensional Saint–Venant solution. The method is derived from a three-dimensional characterization of the beam operators and consists in solving seven particular elasticity problems defined on a longitudinal slice of beam. The computation is immediate when using standard three-dimensional elasticity softs that afford the quadratic 15-node triangular prism element or the 20-node rectangular prism element. The discretization is reduced since only one element is required in the longitudinal direction of the beam. The proposed method is applied to homogeneous and composite beams made of isotropic materials, and to symmetric and antisymmetric laminated beams made of transversely isotropic materials. Structural beam rigidities, elastic couplings, warpings, and three-dimensional stresses are provided and compared to available results.

Keywords: Saint–Venant solution; Beam operators; Finite element method; Shear coefficients; Torsional rigidity; Elastic couplings; Warpings; Shear stresses; Interlaminar stresses; Free-edge effect

1. Introduction

The exact beam theory is established by Ladevèze and Simmonds (1998) for straight elastic beams. It is valid for anisotropic materials, heterogeneous and axially piecewise constant cross-sections, arbitrary loadings, and any shape ratios. The first implementations of this theory (Ladevèze et al., 2001; Sanchez, 2001; El Fatmi and Zenzri, 2002) confirmed and illustrated its pertinence for the analysis of any elastic beams, and particularly composite ones. The use of composite beams is now a real trend in many engineering applications. This trend calls for the development of efficient tools, suitable for the analysis of beams exhibiting three-dimensional effects, for which the classical beam theory assumptions are no more valid. In that purpose, and besides the expensive fully three-dimensional finite element analysis, many

* Corresponding author. Tel.: +216-98-687-001; fax: +216-71-872-729.
E-mail addresses: rached.elfatmi@enit.rnu.tn (R. El Fatmi), hatem.zenzri@enit.rnu.tn (H. Zenzri).

0020-7683/$ - see front matter © 2003 Elsevier Ltd. All rights reserved.
doi:10.1016/j.ijsolstr.2003.12.011

refined beam theories were developed during the last decades (see, e.g., Reddy, 1989; Soldatos and Watson, 1997; Kim and White, 1997; Rand, 2001; Karama et al., 2003, and references therein). All of these theories are built upon simplifying kinematic or static assumptions that cannot be always valid. By contrast, the exact beam theory is free of a priori assumptions, and enables a systematic and inexpensive calculation of non-classical composite effects such as elastic couplings, warpings, and free edge-effects due to the three-dimensional interlaminar stresses (El Fatmi and Zenzri, 2002).

In the exact beam theory, the three-dimensional solution of an equilibrium elasticity beam problem is viewed as the sum of a long wavelength part, called Saint–Venant solution, and a short wavelength part, called the localized solution. The Saint–Venant solution has a fundamental role in the exact beam theory since it constitutes the interior part of the three-dimensional exact solution and it is also needed to evaluate local effects. The expression of the Saint–Venant solution, which is given in Section 2, involves the cross-sectional stress resultants, displacements and rotations, and characteristic beam operators depending on the materials and the cross-section geometry. The cross-sectional stress resultants, displacements, and rotations are solution of a one-dimensional elastic beam problem which includes a characteristic beam compliance operator that describes the structural behavior of the beam. The computation of all the characteristic operators is the principal step in the implementation of the exact beam theory. The numerical method used in Ladevèze et al. (2001) and Sanchez (2001) requires three-dimensional 44-node rectangular prism finite elements of fourth degree. In an earlier method developed by the authors (El Fatmi and Zenzri, 2002), only the cross-section has to be discretized and then only two-dimensional finite elements are needed. However, the two methods are not suited to an immediate use of standard finite element elasticity softs, since in both of them the obtained rigidity matrices are different from those of usual elasticity problems.

The aim of this paper is to simplify the computation of the beam operators in order to allow a larger use of the exact beam theory. In that purpose and starting from the beam operators characterization, established in El Fatmi and Zenzri (2002) and synthetized in Section 3, a three-dimensional formulation of this characterization is derived in Section 4, leading to the determination of the beam operators by a numerical method that can be immediately and inexpensively handled using standard finite element softs. Section 5 is then devoted to illustrations of the exact beam theory using the proposed method to analyse homogeneous and composite beams.

2. Saint–Venant solution and beam operators

The reference problem in the exact beam theory is a three-dimensional equilibrium beam problem. The beam of $\boldsymbol{e}_x$ axis (vectors are highlighted in boldface characters) is occupying a prismatic domain Ω of cross-section S and length L. S_{lat} is the lateral surface and S_0 and S_L are the extremity cross-sections. The materials constituting the beam are linear elastic and the elasticity tensor field is denoted K. The beam is in equilibrium under a body force density $\boldsymbol{f}^{\text{d}}$ on Ω, and surface force densities $\boldsymbol{F}^{\text{d}}$, $\boldsymbol{H}_0$ and $\boldsymbol{H}_L$ on S_{lat}, S_0 and S_L, respectively. The data S, K, $\boldsymbol{f}^{\text{d}}$ and $\boldsymbol{F}^{\text{d}}$ are x-constant. The equations of the reference problem are:

$$\left.\begin{array}{ll} \operatorname{div}\sigma + \boldsymbol{f}^{\text{d}} = \boldsymbol{0} & \text{in } \Omega, \\ \varepsilon(\boldsymbol{\xi}) = \frac{1}{2}(\nabla^{\text{t}}\boldsymbol{\xi} + \nabla\boldsymbol{\xi}) & \text{in } \Omega, \\ \sigma = K : \varepsilon(\boldsymbol{\xi}) & \text{in } \Omega, \\ \sigma \cdot \boldsymbol{n} = \boldsymbol{F}^{\text{d}} & \text{on } S_{\text{lat}} \end{array}\right\} \tag{1}$$

$$\left.\begin{array}{ll} \sigma \cdot (-\boldsymbol{e}_x) = \boldsymbol{H}_0 & \text{on } S_0, \\ \sigma \cdot \boldsymbol{e}_x = \boldsymbol{H}_L & \text{on } S_L, \end{array}\right\} \tag{2}$$

where $\boldsymbol{\xi}$ is the displacement vector, σ is the stress tensor, and $\boldsymbol{n}$ is the unit vector that is normal and external to S_{lat}. The solution of this problem is denoted by $\langle s \rangle = \langle \sigma, \boldsymbol{\xi} \rangle$, where $\boldsymbol{\xi}$ is unique within an arbitrary rigid

body displacement. The Saint–Venant solution, denoted by $\langle s^{sv}\rangle = \langle \sigma^{sv}, \boldsymbol{\xi}^{sv}\rangle$, is the unique x-polynomial solution that exactly satisfies Eq. (1) and satisfies the boundary conditions of Eq. (2) only in terms of resultant (force and moment) of the stresses acting on the extremity cross-sections. Thus, $\langle s^{sv}\rangle$ extends the solution of the well-known Saint–Venant problem in which the beam is isotropic, homogeneous and subjected to only extremity loadings.

As given by Ladevèze and Simmonds (1998), the expression of the Saint–Venant solution is:

$$\left.\begin{array}{l} \boldsymbol{\xi}^{sv} = \boldsymbol{u}(x) + \boldsymbol{\omega}(x) \wedge \boldsymbol{X} + \mathscr{A}(\boldsymbol{X}) \cdot \boldsymbol{T}(x) + \mathscr{B}(\boldsymbol{X}) \cdot \boldsymbol{M}(x) + \boldsymbol{W}^{d}(\boldsymbol{X}), \\ \sigma^{sv} \cdot \boldsymbol{e}_x = \mathscr{A}^{0}(\boldsymbol{X}) \cdot \boldsymbol{T}(x) + \mathscr{B}^{0}(\boldsymbol{X}) \cdot \boldsymbol{M}(x) + \boldsymbol{C}^{d}(\boldsymbol{X}), \end{array}\right\} \tag{3}$$

where $x\boldsymbol{e}_x + \boldsymbol{X}$ denotes the position vector of a point in Ω; $\boldsymbol{X}$ belongs to S. The operators $\mathscr{A}$, $\mathscr{B}$, $\mathscr{A}^0$, $\mathscr{B}^0$, $\boldsymbol{W}^d$ and $\boldsymbol{C}^d$ depend on the materials and the geometry of the cross-section. $\boldsymbol{W}^d$ and $\boldsymbol{C}^d$ are also linearly dependent on the loading $[\boldsymbol{f}^d, \boldsymbol{F}^d]$. $\mathscr{A}^0$, $\mathscr{B}^0$ and $\boldsymbol{C}^d$ are unique and they verify:

$$\left.\begin{array}{l} \int_S \mathscr{A}^0 \,\mathrm{d}S = \int_S \boldsymbol{X} \wedge \mathscr{B}^0 \,\mathrm{d}S = \mathscr{I}, \quad \int_S \mathscr{B}^0 \,\mathrm{d}S = \int_S \boldsymbol{X} \wedge \mathscr{A}^0 \,\mathrm{d}S = O, \\ \int_S \boldsymbol{C}^d \,\mathrm{d}S = \int_S \boldsymbol{X} \wedge \boldsymbol{C}^d \,\mathrm{d}S = \boldsymbol{0}, \end{array}\right\} \tag{4}$$

where $\mathscr{I}$ is the identity tensor and O is the zero tensor. The cross-sectional stress resultants,

$$\boldsymbol{T}(x) = \int_S \sigma \cdot \boldsymbol{e}_x \,\mathrm{d}S = \int_S \sigma^{sv} \cdot \boldsymbol{e}_x \,\mathrm{d}S, \quad \boldsymbol{M}(x) = \int_S \boldsymbol{X} \wedge \sigma \cdot \boldsymbol{e}_x \,\mathrm{d}S = \int_S \boldsymbol{X} \wedge \sigma^{sv} \cdot \boldsymbol{e}_x \,\mathrm{d}S, \tag{5}$$

verify the beam equilibrium equations:

$$\left.\begin{array}{l} \boldsymbol{T}_{,x} + \int_S \boldsymbol{f}^d \,\mathrm{d}S + \int_{\partial S} \boldsymbol{F}^d \,\mathrm{d}\tau = \boldsymbol{o}, \\ \boldsymbol{M}_{,x} + \boldsymbol{e}_x \wedge \boldsymbol{T} + \int_S \boldsymbol{X} \wedge \boldsymbol{f}^d \,\mathrm{d}S + \int_{\partial S} \boldsymbol{X} \wedge \boldsymbol{F}^d \,\mathrm{d}\tau = \boldsymbol{o}, \end{array}\right\} \tag{6}$$

where $(\cdot)_{,x}$ is the derivative with respect to x. The operators $\mathscr{A}$, $\mathscr{B}$ and $\boldsymbol{W}^d$ are taken such as:

$$\left.\begin{array}{l} \int_S \mathscr{A}^{0T} \cdot \mathscr{A} \,\mathrm{d}S = \int_S \mathscr{A}^{0T} \cdot \mathscr{B} \,\mathrm{d}S = \int_S \mathscr{B}^{0T} \cdot \mathscr{A} \,\mathrm{d}S = \int_S \mathscr{B}^{0T} \cdot \mathscr{B} \,\mathrm{d}S = O, \\ \int_S \left(\mathscr{A}^{0T} \cdot \boldsymbol{W}^d - \mathscr{A}^{T} \cdot \boldsymbol{C}^d\right) \mathrm{d}S = \boldsymbol{0}, \quad \int_S \left(\mathscr{B}^{0T} \cdot \boldsymbol{W}^d - \mathscr{B}^{T} \cdot \boldsymbol{C}^d\right) \mathrm{d}S = \boldsymbol{0}, \end{array}\right\} \tag{7}$$

where $(\cdot)^T$ is the transpose operator. The conditions of Eq. (7) are always possible, since $\boldsymbol{\xi}^{sv}$ is unique within an arbitrary rigid body displacement, and they lead to cross-sectional displacement, $\boldsymbol{u}$, and rotation, $\boldsymbol{\omega}$, which verify:

$$\left.\begin{array}{l} \boldsymbol{u}(x) = \int_S \left(\mathscr{A}^{0T} \cdot \boldsymbol{\xi} - \mathscr{A}^{T} \cdot (\sigma \cdot \boldsymbol{e}_x)\right) \mathrm{d}S = \int_S \left(\mathscr{A}^{0T} \cdot \boldsymbol{\xi}^{sv} - \mathscr{A}^{T} \cdot (\sigma^{sv} \cdot \boldsymbol{e}_x)\right) \mathrm{d}S, \\ \boldsymbol{\omega}(x) = \int_S \left(\mathscr{B}^{0T} \cdot \boldsymbol{\xi} - \mathscr{B}^{T} \cdot (\sigma \cdot \boldsymbol{e}_x)\right) \mathrm{d}S = \int_S \left(\mathscr{B}^{0T} \cdot \boldsymbol{\xi}^{sv} - \mathscr{B}^{T} \cdot (\sigma^{sv} \cdot \boldsymbol{e}_x)\right) \mathrm{d}S. \end{array}\right\} \tag{8}$$

The cross-sectional strains $\boldsymbol{\gamma} = \boldsymbol{u}_{,x} + \boldsymbol{e}_x \wedge \boldsymbol{\omega}$ and $\boldsymbol{\chi} = \boldsymbol{\omega}_{,x}$ are related to the stress resultants by the following one-dimensional structural behavior equation:

$$\begin{bmatrix} \boldsymbol{\gamma} \\ \boldsymbol{\chi} \end{bmatrix} = [\Lambda] \begin{bmatrix} \boldsymbol{T} \\ \boldsymbol{M} \end{bmatrix} + \begin{bmatrix} \boldsymbol{\gamma}^d \\ \boldsymbol{\chi}^d \end{bmatrix}, \quad \left\{\begin{array}{l} \boldsymbol{\gamma}^d = \int_S \mathscr{A}^{T} \cdot \boldsymbol{f}^d \,\mathrm{d}S + \int_{\partial S} \mathscr{A}^{T} \cdot \boldsymbol{F}^d \,\mathrm{d}\tau, \\ \boldsymbol{\chi}^d = \int_S \mathscr{B}^{T} \cdot \boldsymbol{f}^d \,\mathrm{d}S + \int_{\partial S} \mathscr{B}^{T} \cdot \boldsymbol{F}^d \,\mathrm{d}\tau. \end{array}\right. \tag{9}$$

The structural compliance operator of the beam, Λ, is symmetric, definite, positive, and depends on the materials and the geometry of the cross-section. Eqs. (6) and (9) and boundary conditions on S_0 and S_L, form the one-dimensional problem of the exact elastic beam theory. The exactitude of this theory follows from Eqs. (5) and (8) which show that the cross-sectional stress resultants, displacements and rotations defined on the exact solution $\langle s\rangle$ coincide with those of the Saint–Venant solution $\langle s^{sv}\rangle$; then the compliance operator Λ is also exact. For a non-x-constant loading $[\boldsymbol{f}^d(x), \boldsymbol{F}^d(x)]$, the Saint–Venant solution and the one-dimensional problem are also defined by Eqs. (3) and (9), except that the values of $\boldsymbol{W}^d$, $\boldsymbol{C}^d$, $\boldsymbol{\gamma}^d$ and $\boldsymbol{\chi}^d$ become dependent on x. For such non-x-constant loading, Ladevèze and Simmonds (1998) proved that the

Saint–Venant solution remains an interior solution of the three-dimensional equilibrium beam problem and they also proved that Eqs. (5) and (8) are still verified.

3. Characterization of the beam operators

In a previous work the authors established that the beam operators can be determined by the minimization of seven functionals derived from the potential energies associated to seven elasticity problems (El Fatmi and Zenzri, 2002). In each of these problems, the loading is taken such as the exact solution, $\langle s \rangle$, coincide with that of Saint–Venant, $\langle s^{sv} \rangle$. The first six problems are problems of traction, torque, bendings and shear forces. They allow the determination of $\mathscr{A}$, $\mathscr{B}$, $\mathscr{A}^0$, $\mathscr{B}^0$ and Λ. For a given loading $[\boldsymbol{f}^d, \boldsymbol{F}^d]$, a seventh problem is devoted to the determination of $\boldsymbol{W}^d$ and $\boldsymbol{C}^d$. The main results of El Fatmi and Zenzri (2002) are synthesized in the following proposition.

Notations

$$\mathscr{A} = [\boldsymbol{U}^1, \boldsymbol{U}^2, \boldsymbol{U}^3], \quad \mathscr{B} = [\boldsymbol{U}^4, \boldsymbol{U}^5, \boldsymbol{U}^6], \quad \mathscr{A}^0 = [\boldsymbol{C}^1, \boldsymbol{C}^2, \boldsymbol{C}^3], \quad \mathscr{B}^0 = [\boldsymbol{C}^4, \boldsymbol{C}^5, \boldsymbol{C}^6],$$

$$f^1\boldsymbol{e}_x + f^2\boldsymbol{e}_y + f^3\boldsymbol{e}_z = \int_S \boldsymbol{f}^d \, dS + \int_{\partial S} \boldsymbol{F}^d \, d\tau,$$
$$f^4\boldsymbol{e}_x + f^5\boldsymbol{e}_y + f^6\boldsymbol{e}_z = \int_S \boldsymbol{X} \wedge \boldsymbol{f}^d \, dS + \int_{\partial S} \boldsymbol{X} \wedge \boldsymbol{F}^d \, d\tau,$$

$$\boldsymbol{\lambda}^* = \begin{bmatrix} \lambda_1^* \\ \lambda_4^* \\ \lambda_5^* \\ \lambda_6^* \end{bmatrix}, \quad \boldsymbol{V}^* = \boldsymbol{V}^*(y,z), \quad \bar{\boldsymbol{\xi}}^*(\boldsymbol{\lambda}^*, \boldsymbol{V}^*) = \begin{bmatrix} \lambda_1^* x + \lambda_5^* xz - \lambda_6^* xy + V_x^* \\ \frac{1}{2}\lambda_6^* x^2 - \lambda_4^* xz + V_y^* \\ -\frac{1}{2}\lambda_5^* x^2 + \lambda_4^* xy + V_z^* \end{bmatrix}, \tag{10}$$

$$D(\boldsymbol{V}^*) = \tfrac{1}{2}(\boldsymbol{e}_x \otimes \boldsymbol{V}^* + \boldsymbol{V}^* \otimes \boldsymbol{e}_x), \quad \boldsymbol{\alpha}^* = -\int_S \mathscr{B}^{0T} \cdot \boldsymbol{V}^* \, dS, \quad \boldsymbol{\beta}^* = -\int_S \mathscr{A}^{0T} \cdot \boldsymbol{V}^* \, dS, \tag{11}$$

where $(\boldsymbol{e}_x, \boldsymbol{e}_y, \boldsymbol{e}_z)$ is an orthonormal base and $\otimes$ is the tensorial product operator.

Proposition. *The minimisation of the functionals:*

$$J^k(\bar{\boldsymbol{\xi}}^*(\boldsymbol{\lambda}^*, \boldsymbol{V}^*)) = \frac{L}{2}\int_S \varepsilon(\bar{\boldsymbol{\xi}}^*) : K : \varepsilon(\bar{\boldsymbol{\xi}}^*) \, dS - \mathscr{L}^k(\bar{\boldsymbol{\xi}}^*), \quad k = 1, \ldots, 6, d, \tag{12}$$

where the linear form $\mathscr{L}^k$ are:

$$\left.\begin{aligned} &\mathscr{L}^k = L\lambda_k^*, \quad k = 1,4,5,6, \\ &\mathscr{L}^2 = L\int_S \left[\varepsilon(\bar{\boldsymbol{\xi}}^*) : K : D(\boldsymbol{U}^6 - \beta_y^6\boldsymbol{e}_y - \beta_z^6\boldsymbol{e}_z) - \boldsymbol{C}^6 \cdot \boldsymbol{V}^*\right] dS, \\ &\mathscr{L}^3 = -L\int_S \left[\varepsilon(\bar{\boldsymbol{\xi}}^*) : K : D(\boldsymbol{U}^5 - \beta_y^5\boldsymbol{e}_y - \beta_z^5\boldsymbol{e}_z) - \boldsymbol{C}^5 \cdot \boldsymbol{V}^*\right] dS, \\ &\mathscr{L}^d = L\int_S \left[\varepsilon(\bar{\boldsymbol{\xi}}^*) : K : \textstyle\sum_{i=1}^6 f^i D(\boldsymbol{U}^i) + \left(\boldsymbol{f}^d - \sum_{i=1}^6 f^i \boldsymbol{C}^i\right) \cdot \boldsymbol{V}^*\right] dS + L\int_{\partial S} \boldsymbol{F}^d \cdot \boldsymbol{V}^* \, d\tau, \end{aligned}\right\} \tag{13}$$

leads to the beam operators as follows:

- *For $k = 1,4,5,6$ and $\bar{\boldsymbol{\xi}}^k(\boldsymbol{\lambda}^k, \boldsymbol{V}^k)$ minimising J^k, we have:*

$$\left.\begin{aligned} &\boldsymbol{C}^k = K : \varepsilon(\bar{\boldsymbol{\xi}}^k) \cdot \boldsymbol{e}_x, \quad \boldsymbol{U}^k = \boldsymbol{V}^k + \boldsymbol{\beta}^k + \boldsymbol{\alpha}^k \wedge \boldsymbol{X}, \\ &\Lambda_{ik} = \lambda_i^k \ (i = 1,4,5,6), \quad \Lambda_{2k} = \alpha_z^k, \quad \Lambda_{3k} = -\alpha_y^k. \end{aligned}\right\} \tag{14}$$

- *For* $\bar{\boldsymbol{\xi}}^2(\boldsymbol{\lambda}^2, \boldsymbol{V}^2)$ *minimising* J^2*, we have:*

$$\left.\begin{aligned} &\boldsymbol{C}^2 = K : \left[\varepsilon(\bar{\boldsymbol{\xi}}^2) - D(\boldsymbol{U}^6 - \beta_y^6 \boldsymbol{e}_y - \beta_z^6 \boldsymbol{e}_z)\right] \cdot \boldsymbol{e}_x, \\ &\boldsymbol{U}^2 = \boldsymbol{V}^2 + \boldsymbol{\beta}^2 + \boldsymbol{\alpha}^2 \wedge \boldsymbol{X}, \quad \Lambda_{22} = \beta_y^6 + \alpha_z^2, \quad \Lambda_{32} = \beta_z^6 - \alpha_y^6. \end{aligned}\right\} \tag{15}$$

- *For* $\bar{\boldsymbol{\xi}}^3(\boldsymbol{\lambda}^3, \boldsymbol{V}^3)$ *minimising* J^3*, we have:*

$$\left.\begin{aligned} &\boldsymbol{C}^3 = K : \left[\varepsilon(\bar{\boldsymbol{\xi}}^3) + D(\boldsymbol{U}^5 - \beta_y^5 \boldsymbol{e}_y - \beta_z^5 \boldsymbol{e}_z)\right] \cdot \boldsymbol{e}_x, \\ &\boldsymbol{U}^3 = \boldsymbol{V}^3 + \boldsymbol{\beta}^3 + \boldsymbol{\alpha}^3 \wedge \boldsymbol{X}, \quad \Lambda_{23} = -\beta_y^5 + \alpha_z^3, \quad \Lambda_{33} = -\beta_z^5 - \alpha_y^3. \end{aligned}\right\} \tag{16}$$

- *For* $\bar{\boldsymbol{\xi}}^{\mathrm{d}}(\boldsymbol{\lambda}^{\mathrm{d}}, \boldsymbol{V}^{\mathrm{d}})$ *minimising* J^{d}*, we have:*

$$\left.\begin{aligned} &\boldsymbol{C}^{\mathrm{d}} = K : [\varepsilon(\bar{\boldsymbol{\xi}}^{\mathrm{d}}) - \textstyle\sum_{i=1}^{6} f^i D(\boldsymbol{U}^i)] \cdot \boldsymbol{e}_x, \\ &\boldsymbol{W}^{\mathrm{d}} = \boldsymbol{V}^{\mathrm{d}} + \boldsymbol{\beta}^{\mathrm{d}} + \textstyle\int_S \mathscr{A}^{\mathrm{T}} \cdot \boldsymbol{C}^{\mathrm{d}} \,\mathrm{d}S + (\boldsymbol{\alpha}^{\mathrm{d}} + \int_S \mathscr{B}^{\mathrm{T}} \cdot \boldsymbol{C}^{\mathrm{d}} \,\mathrm{d}S) \wedge \boldsymbol{X}. \end{aligned}\right\} \tag{17}$$

El Fatmi and Zenzri (2002) performed the minimisation of the functionals J^k by using a two-dimensional finite element method where the unknown are the scalars λ_i^k and the degrees of freedom of the fields $\boldsymbol{V}^k$. The computation is economical since only the cross-section has to be discretized, but the rigidity matrix is different from the two-dimensional elasticity matrices. Thus, the implementation of this method within available softs needs the introduction of a new finite element model. Such work can be avoided by the use of a three-dimensional formulation of the beam operators characterization. The three-dimensional calculations have also the advantage of being more appropriate to the study of localized effects which are completely three-dimensional.

4. Three-dimensional characterization and numerical method

Using the form of the fields $\bar{\boldsymbol{\xi}}^*$ (Eq. (10)), which especially leads to x-constant strain tensors $\varepsilon(\bar{\boldsymbol{\xi}}^*(\boldsymbol{\lambda}^*, \mathbf{V}^*))$, the following expressions of the functionals J^k and the linear forms $\mathscr{L}^k$, can be easily derived from Eqs. (12) and (13):

$$J^k(\bar{\boldsymbol{\xi}}^*) = \frac{1}{2}\int_\Omega \varepsilon(\bar{\boldsymbol{\xi}}^*) : K : \varepsilon(\bar{\boldsymbol{\xi}}^*)\,\mathrm{d}\Omega - \mathscr{L}^k(\bar{\boldsymbol{\xi}}^*), \quad k = 1, \ldots, 6, d, \tag{18}$$

$$\left.\begin{aligned} &\mathscr{L}^1 = \tfrac{1}{S}\left(\textstyle\int_{S_L} \bar{\boldsymbol{\xi}}^* \cdot \mathbf{e}_x \,\mathrm{d}S - \int_{S_0} \bar{\boldsymbol{\xi}}^* \cdot \mathbf{e}_x \,\mathrm{d}S\right), \\ &\mathscr{L}^4 = \tfrac{1}{I}\left(\textstyle\int_{S_L} \bar{\boldsymbol{\xi}}^* \cdot (\mathbf{e}_x \wedge \mathbf{X})\,\mathrm{d}S \int_{S_0} \bar{\boldsymbol{\xi}}^* \cdot (\mathbf{e}_x \wedge \mathbf{X})\,\mathrm{d}S\right), \quad I = \textstyle\int_S \mathbf{X} \cdot \mathbf{X}\,\mathrm{d}S, \\ &\mathscr{L}^5 = -\tfrac{2}{SL}\left(\textstyle\int_{S_L} \bar{\boldsymbol{\xi}}^* \cdot \mathbf{e}_z \,\mathrm{d}S - \int_{S_0} \bar{\boldsymbol{\xi}}^* \cdot \mathbf{e}_z \,\mathrm{d}S\right), \\ &\mathscr{L}^6 = \tfrac{2}{SL}\left(\textstyle\int_{S_L} \bar{\boldsymbol{\xi}}^* \cdot \mathbf{e}_y \,\mathrm{d}S - \int_{S_0} \bar{\boldsymbol{\xi}}^* \cdot \mathbf{e}_y \,\mathrm{d}S\right), \\ &\mathscr{L}^2 = \textstyle\int_\Omega \varepsilon(\bar{\boldsymbol{\xi}}^*) : K : D\left(\mathbf{U}^6 - \beta_y^6 \mathbf{e}_y - \beta_z^6 \mathbf{e}_z\right)\mathrm{d}\Omega - L\int_{S_0} \bar{\boldsymbol{\xi}}^* \cdot \mathbf{C}^6\,\mathrm{d}S, \\ &\mathscr{L}^3 = -\textstyle\int_\Omega \varepsilon(\bar{\boldsymbol{\xi}}^*) : K : D\left(\mathbf{U}^5 - \beta_y^5 \mathbf{e}_y - \beta_z^5 \mathbf{e}_z\right)\mathrm{d}\Omega + L\int_{S_0} \bar{\boldsymbol{\xi}}^* \cdot \mathbf{C}^5\,\mathrm{d}S, \\ &\mathscr{L}^{\mathrm{d}} = \textstyle\int_\Omega \varepsilon(\bar{\boldsymbol{\xi}}^*) : K : \sum_{i=1}^{6} f^i D(\mathbf{U}^i)\,\mathrm{d}\Omega + L\int_{S_0} \bar{\boldsymbol{\xi}}^* \cdot \left(\mathbf{f}^{\mathrm{d}} - \sum_{i=1}^{6} f^i \mathbf{C}^i\right)\mathrm{d}S + L\int_{\partial S_0} \bar{\boldsymbol{\xi}}^* \cdot \mathbf{F}^{\mathrm{d}}\,\mathrm{d}\tau. \end{aligned}\right\} \tag{19}$$

To obtain Eq. (19), the axis of the beam is supposed to go through the geometric centers of the cross-sections so that: $\int_S y\,\mathrm{d}S = \int_S z\,\mathrm{d}S = 0$.

In the expressions of the linear forms $\mathscr{L}^k$ (Eq. (19)), the variables $\boldsymbol{\lambda}^*$ and $\boldsymbol{V}^*$ do not appear explicitly; the only variable is now the displacement field $\bar{\boldsymbol{\xi}}^*$. Thus, the problem of determining a field $\bar{\boldsymbol{\xi}}^k$ minimising a

functional J^k, appears as a displacement formulation of an equilibrium problem in which the elastic beam occupying the three-dimensional domain Ω is submitted to a loading defined by the linear form $\mathscr{L}^k$. Then, the three-dimensional finite element method is obviously appropriated to the numerical computation of the fields $\bar{\boldsymbol{\xi}}^k$. Since these $\bar{\boldsymbol{\xi}}^k$ fields are quadratic relatively to the x coordinate (Eq. (10)), the quadratic 15-node triangular prism element and the 20-node rectangular prism element are, among the common finite elements, the most suitable to the $\bar{\boldsymbol{\xi}}^k$ computation. And it is clear that in the x direction only one element has to be used, whereas the cross-section should be discretized as necessary.

To ensure the conformity of this finite element method with the vectorial space of the fields $\bar{\boldsymbol{\xi}}^*$, relations must be imposed between the degrees of freedom of each element. There are 23 relations for the 15-node element and 32 relations for the 20-node element. These relations, given in Appendix A for the reference finite elements, are easily obtained by setting the coefficients of the x-monomials in the finite element basis functions in accordance with those of Eq. (10). These coefficients also must be constant within all the elements; however, the continuity of the base functions of the finite element space and the 23 or 32 imposed relations make this condition automatically satisfied.

The chararacteristic beam operators are derived from the solutions $\bar{\boldsymbol{\xi}}^k$ as given in Eqs. (14)–(17), in which the vectors $\boldsymbol{V}^k$ are just the vectors $\bar{\boldsymbol{\xi}}^k_{|S_0}$. In Eq. (14), the components of the compliance operator may also be obtained by:

$$\Lambda_{ik} = \frac{1}{L}\int_{\Omega} \varepsilon(\bar{\boldsymbol{\xi}}^i) : K : \varepsilon(\bar{\boldsymbol{\xi}}^k)\,\mathrm{d}\Omega \quad \forall i = 1,\ldots,6 \quad \text{and} \quad \forall k = 1,4,5,6. \tag{20}$$

As shown in Eq. (18), the seven problems are solved using the same rigidity matrix. However, the minimisations of J^1, J^4, J^5 and J^6 must be done before those of J^2 and J^3; and, for a given loading $[\boldsymbol{f}^{\mathrm{d}}, \boldsymbol{F}^{\mathrm{d}}]$, the minimisation of J^{d} must be preceded by the resolution of the six other problems.

5. Applications

The numerical method presented in the previous section is implemented within the finite element soft Castem2000 (Le Fichoux, 1998). For given cross-sectional geometry and materials, the operators $\mathscr{A}^0, \mathscr{B}^0, \mathscr{A}, \mathscr{B}$ and Λ are computed. From these operators, three-dimensional stresses and displacements, $\langle \sigma^{\mathrm{sv}}, \boldsymbol{\xi}^{\mathrm{sv}} \rangle$, can be derived for any cross-section subjected to internal forces $(\boldsymbol{T}, \boldsymbol{M})$.

5.1. Homogeneous isotropic beams

The first applications are devoted to the analysis of the structural behavior of homogeneous cross-sections made of isotropic materials. For such cross-sections, the compliance operator Λ can be derived from the solution of the classical Saint–Venant problem. Relatively to the (G, y, z) system of coordinates, where G is the geometric center of the cross-section and (y, z) are its principal axes, the components of Λ are classically expressed as follows:

$$[\Lambda] = \begin{bmatrix} \frac{1}{ES} & 0 & 0 & 0 & 0 & 0 \\ 0 & \frac{z_c^2}{GJ} + \frac{1}{k_y GS} & \Lambda_{23} & \Lambda_{24} & 0 & 0 \\ 0 & \Lambda_{23} & \frac{y_c^2}{GJ} + \frac{1}{k_z GS} & \Lambda_{34} & 0 & 0 \\ 0 & \Lambda_{24} & \Lambda_{34} & \frac{1}{GJ} & 0 & 0 \\ 0 & 0 & 0 & 0 & \frac{1}{EI_y} & 0 \\ 0 & 0 & 0 & 0 & 0 & \frac{1}{EI_z} \end{bmatrix}, \tag{21}$$

where E is the Young's modulus; $G = E/2(1+\nu)$, the shear modulus; ν, the Poisson's coefficient; (I_y, I_z), the principal inertias of the cross-section; (k_y, k_z), the shear coefficients; (y_c, z_c), the coordinates of the shear center C and J is the torsional constant. For an y–z-symmetrical cross-section, C and G coincide and the matrix $[\Lambda]$ is diagonal. For a non-symmetrical cross-section the following approximations are commonly used:

$$\Lambda_{23} = -\frac{y_c z_c}{GJ}, \quad \Lambda_{24} = \frac{z_c}{GJ}, \quad \Lambda_{34} = -\frac{y_c}{GJ}. \tag{22}$$

Except for particular cross-sections, such as the circular ones where analytical expressions are available, the computation of J and (k_y, k_z) is generally handled using a two-dimensional finite element method or one of the numerous simplified methods (see, e.g, Batoz and Dhatt, 1990).

Table 1 provides, for five cross-sections denoted $S1$, $S2$, $S3$, $S4$ and $S5$, a comparison between the numerical results obtained by the current method and those available in the literature. This comparison

Table 1
Torsional contant (J), shear coefficients (k_y, k_z) and position (z_c) of the shear center for homogeneous isotropic cross-sections (comparison between current and available results)

Cross-sections		Present results			Available results		
S1 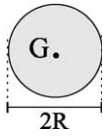	J/R^4		1.56			1.57	
	ν	0	0.3	0.45	0	0.3	0.45
	k	0.853	0.846	0.841	0.857	0.850	0.846
S2 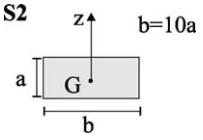	J/b^4		3.124×10^{-4}			3.123×10^{-4}	
	ν	0	0.3	0.45	0	0.3	0.45
	k_y	0.833	0.833	0.833	0.833	0.833	0.833
	k_z	0.833	0.179	0.110	0.833	0.179	0.110
S3 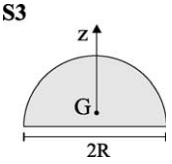	J/R^4		0.295			0.294	
	z_c/R		0.0838			0.0869	
	ν	0	0.3	0.45	0.3		
	k_y	0.853	0.853	0.853	0.873		
	k_z	0.763	0.730	0.706	0.771		
S4 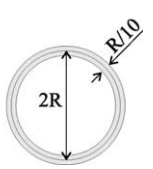	J/R^4		0.6230			0.6299	
	ν	0	0.3	0.45	0	0.3	0.45
	k	0.499	0.499	0.499	0.502	0.502	0.502
S5 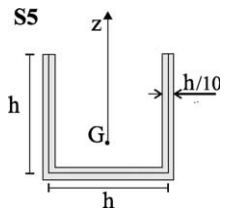	J/h^4		9.96×10^{-4}			10×10^{-4}	
	z_c/h		0.0752			0.0762	
	ν		0				
	k_y		0.236			0.223	
	k_z		0.537			0.513	

concerns the shear coefficients (k_y, k_z), the torsional constant J and the shear center coordinate (z_c). When using the current method, the geometrical discretization of the cross-sections is made by 15-node triangular prism elements for $S1$, $S3$ and $S4$ and 20-node rectangular prism elements for $S2$ and $S5$. In each case the cross-section is divided into about one hundred elements.

For the circular cross-section $S1$ and the circular tube $S4$, the current results are in accordance with the analytical expressions $J = \frac{\pi}{2}(b^4 - a^4)$ and $k_y = k_z = k = \frac{6(a^2+b^2)^2(1+\nu)^2}{(a^4+b^4)(7+14\nu+8\nu^2)+2a^2b^2(17+34\nu+16\nu^2)}$ where a is the inner radius and b is the outer radius (Renton, 1997). Using the exact beam theory, the case of rectangular cross-sections was recently reviewed by Sanchez (2001) who confirmed the results of Renton (1991) concerning the dependency of the shear coefficients on the Poisson's coefficient and the geometrical ratio of the cross-section; for the rectangular cross-section $S2$ the current results conform naturally to those of Sanchez (2001). For the non-symmetric cross-sections $S3$ and $S5$, the numerically obtained matrix $[\Lambda]$ has the shape given in Eq. (21) and it verifies the approximations written in Eq. (22). For the semi-circular cross-section $S3$, the present results are compared with those obtained by Friedman and Kosmatka (2000) using the boundary element method. For $S5$, the current results are in accordance with those obtained by the classical theory of open thin walled cross-sections (Vlassov, 1962).

5.2. Composite beams made of isotropic materials

The composite cross-sections presented in Table 2 are made of two isotropical materials. The computations also concern the structural behavior. Current results are here compared to those derived from the common simplified composite beam theory which is described, for example, by Gay (1998) and Batoz and Dhatt (1990). This theory is based on a kinematic approach and uses the static assumptions: $(\sigma_{yy}, \sigma_{zz}, \sigma_{yz}) \ll \sigma_{xx}$. It leads to a structural compliance beam operator that has the same couplings as the homogeneous case when it is expressed relatively to the (G^e, y, z) system of coordinates, where G^e is the elastic center of the cross-section and (y, z) are its principal axes:

$$\int_S [Ey, Ez, Eyz]\,\mathrm{d}S = [0, 0, 0]. \tag{23}$$

The components of this simplified operator, denoted Λ^S, are as follows:

$$[\Lambda^S] = \begin{bmatrix} \frac{1}{\widetilde{ES}} & 0 & 0 & 0 & 0 & 0 \\ 0 & \frac{z_c^2}{\widetilde{GJ}} + \frac{1}{k_y \widetilde{GS}} & -\frac{y_c z_c}{\widetilde{GJ}} & \frac{z_c}{\widetilde{GJ}} & 0 & 0 \\ 0 & -\frac{y_c z_c}{\widetilde{GJ}} & \frac{y_c^2}{\widetilde{GJ}} + \frac{1}{k_z \widetilde{GS}} & -\frac{y_c}{\widetilde{GJ}} & 0 & 0 \\ 0 & \frac{z_c}{\widetilde{GJ}} & -\frac{y_c}{\widetilde{GJ}} & \frac{1}{\widetilde{GJ}} & 0 & 0 \\ 0 & 0 & 0 & 0 & \frac{1}{\widetilde{EI_y}} & 0 \\ 0 & 0 & 0 & 0 & 0 & \frac{1}{\widetilde{EI_z}} \end{bmatrix}, \tag{24}$$

where

$$\left[\widetilde{ES}, \widetilde{GS}, \widetilde{EI_y}, \widetilde{EI_z}\right] = \int_S [E, G, Ez^2, Ey^2]\,\mathrm{d}S. \tag{25}$$

The determination of the homogenised torsional rigidity $\widetilde{GJ}$, the shear coefficients (k_y, k_z) and the (y_c, z_c) shear center coordinates also needs two-dimensional finite element computations which may be supplied by many available softs. For the cross-sections $S6$, $S7$, $S8$ and $S9$, described in Table 2, these computations are obtained using the RDM5 soft (Debard, 1997) and are compared to those derived from the components of

Table 2
Torsional rigidity ($\widetilde{GJ}$), shear coefficients (k_y, k_z) and position (y_c, z_c) of the shear center for composite cross-sections made by isotropic materials (comparison between current and available results)

Cross-sections			Present results	Available results
S6 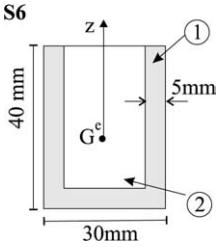	$E_1 = 72.95$ GPa $G_1 = 27.51$ GPa $E_2 = 10.67$ GPa $G_2 = 4.02$ GPa ($v_1 = v_2 = 0.33$)	$\widetilde{GJ}/(GJ)_1$ k_y k_z z_c	0.5249 0.428 0.727 −4.90	0.5252 0.430 0.729 −4.89
S7 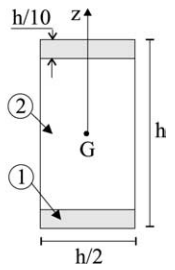	(a) $E_1/E_2 = 50$ $v_1 = 0, v_2 = 0$ (b) $E_1/E_2 = 50$ $v_1 = 0, v_2 = 0.45$ (c) $E_1/E_2 = 1$ $v_1, = 0, v_2 = 0.45$	$\widetilde{GJ}/(GJ)_1$ k_y k_z $\widetilde{GJ}/(GJ)_1$ k_y k_z $\widetilde{GJ}/(GJ)_1$ k_y k_z	0.0395 0.833 0.094 0.0307 0.773 0.069 0.747 0.728 0.769	0.0395 0.833 0.094 0.0307 0.829 0.069 0.747 0.827 0.770
S8 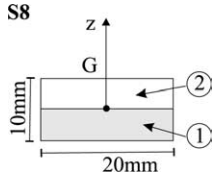	$E_1 = E_2 = 1$ GPa $v_1 = 0$ $v_2 = 0.45$	$\widetilde{GJ}/(GJ)_1$ k_y k_z z_c (mm)	0.8251 0.826 0.774 −0.723	0.8295 0.829 0.807 −0.704
S9 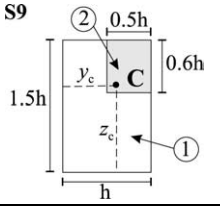	$E_2/E_1 = 10$ $v_1 = 0.1, v_2 = 0.3$	$\widetilde{GJ}/(GJ)_1$ k_y k_z y_c/h Z_c/h	1.5314 0.517 0.668 0.576 0.941	1.5317 0.516 0.673 0.580 0.944

the exact beam theory operator Λ computed in the same (G^e, y, z) coordinates system. When using the current method for the computation of the Λ components, the geometrical discretization, for $S6$, $S7$, $S8$ and $S9$, is made by 20-node rectangular prism elements. In each case the cross-section is divided into about two hundreds elements and the computation time is about one minute on a pentium 4 microcomputer. When using the RDM5 soft, the same computation time is nearly needed.

In Table 2 and for each cross-section $Si(i = 6, 7, 8, 9)$ made of the materials 1 and 2, the homogenised torsional rigidity $\widetilde{GJ}$ is normalized by the torsional rigidity $(GJ)_1$ of the homogeneous cross-section made by material 1 and having the geometry of Si. For $S6$ and $S7$, the current results show that the matrix $[\Lambda]$ has

numerically the same shape as $[\Lambda^S]$. The equalities written in Eq. (25) are also numerically verified by the components of $[\Lambda]$. The example $S6$ is taken from a previously published work (Pastor, 2000) in which only the torsional rigidity was studied. This study is based on kinematic and static approachs and two-dimensional finite element method. It leaded to the following bounding: $0.5247 < \frac{\widetilde{GJ}}{(GJ)_1} < 0.5253$. This bounding is here confirmed. In $S6$ and $S7(a)$, the materials have the same Poisson's coefficients ($v_1 = v_2$) and the current results confirm those of the simplified theory. However, for the cross-sections $S7(b)$, $S7(c)$ and $S8$, which have an important Poisson's coefficients contrast, a significant difference between the compared results is detected in the values of the shear coefficient k_y. This difference is predictable since the static assumption $(\sigma_{yy}, \sigma_{zz}, \sigma_{yz}) \ll \sigma_{xx}$ used in the simplified theory is not valid for such material contrast. Moreover, for the cross-section $S8$, which is not symmetric with respect to the y-axis because of the Poisson's coefficients contrast, the shape of the matrix $[\Lambda]$ is different from that of $[\Lambda^S]$ given in Eq. (24). The numerical values of the $[\Lambda]$ components, which are as follows:

$$[\Lambda] = 10^{(-6)} \begin{bmatrix} 4.94093 & 0 & 0 & 0 & 1.93333 & 0 \\ 0 & 14.6051 & 0 & -383.134 & 0 & 0 \\ 0 & 0 & 15.2937 & 0 & 0 & 0 \\ 0 & -383.134 & 0 & 529950 & 0 & 0 \\ 1.93333 & 0 & 0 & 0 & 594610 & 0 \\ 0 & 0 & 0 & 0 & 0 & 148690 \end{bmatrix}, \tag{26}$$

show that the cross-section $S8$ exhibits elastic coupling, between extension and y-bending, which is not detected by the simplified theory. In Eq. (26), $\Lambda_{11}, \Lambda_{22}$ and Λ_{33} are expressed in N^{-1}, $\Lambda_{44}, \Lambda_{55}$ and Λ_{66} are in $\mathrm{N}^{-1}\,\mathrm{m}^{-1}$ and Λ_{15} and Λ_{24} are in $\mathrm{N}^{-1}\,\mathrm{m}^{-1}$. For the unsymmetric cross-section $S9$, the numerical values of the $[\Lambda]$ components also show that $S9$ exhibits elastic couplings between extension and the y and z bendings.

5.3. Laminated composite beams made of transversely isotropic materials

In the examples presented hereafter, symmetric and antisymmetric cross-sections consisting of four transversely isotropic laminae are studied. The considered lamination modes are: $[0, \pm\theta, \theta, 0]$, where θ is the angle of the ply with respect to the longitudinal axis. The material properties are typical for graphite/epoxy and are as follows:

Young's moduli

$$E_1 = 137.6 \text{ GPa}, \quad E_2 = E_3 = 14.448 \text{ GPa}$$

Shear moduli

$$G_{12} = G_{13} = G_{23} = 5.848 \text{ GPa}$$

Poisson's ratios

$$v_{12} = v_{13} = v_{23} = 0.21$$

where the subscript 1 refers to the graphite fiber direction. The rectangular cross-sectional area is assumed to be bounded by the lines $y = \pm a$ and $z = \pm b = \pm a/2$, and the four laminae are of identical thickness, $h = b/4$ (Fig. 1). The geometrical discretization is made by 20-node rectangular prism elements where the cross-section is divided into 392 rectangles. (As in any finite element elasticity analysis, to achieve a required accuracy, defined by an error estimator, an adaptative procedure has to be used to determine the suitable number of elements (see, e.g., Zienkiewicz et al., 1989; Batoz and Dhatt, 1990)).

The numerically obtained structural compliances Λ_{ij}, expressed relatively to the (G, y, z) coordinates system, show that the elastic couplings in the symmetric cross-sections are of "extension-bending" ($\Lambda_{12} \neq 0$)

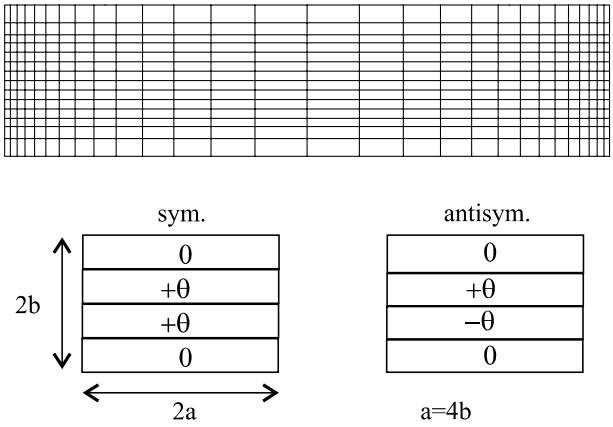

Fig. 1. Geometry and mesh of the symmetric and antisymmetric cross-sections.

and "bending-twist" ($\Lambda_{45} \neq 0$) whereas they are of "extension-twist" ($\Lambda_{14} \neq 0$) and "y–z-bendings" ($\Lambda_{25} \neq 0$) in the antisymmetric cross-sections.

The compliances associated to these couplings are presented in Figs. 2 and 3 as functions of θ. The "extension-bending" and "extension-twist" couplings are also illustrated in Fig. 4 which presents the Saint–Venant deformations of the beams $[0, \pm 30, 30, 0]$ under traction. The warpings and the in-plane deformations, presented in Fig. 5 and corresponding to the contributions of each of the six beam internal forces, follow from the computation of the operators $\mathscr{A}$ and $\mathscr{B}$ as follows:

$$\left.\begin{aligned} \boldsymbol{\xi}^{\mathrm{sv}}_{\mathrm{warping}} &= ((\mathscr{A}(\boldsymbol{X}) \cdot \boldsymbol{T}(x) + \mathscr{B}(\boldsymbol{X}) \cdot \boldsymbol{M}(x)) \cdot \boldsymbol{e}_x)\boldsymbol{e}_x, \\ \boldsymbol{\xi}^{\mathrm{sv}}_{\mathrm{in-plane}} &= \mathscr{A}(\boldsymbol{X}) \cdot \boldsymbol{T}(x) + \mathscr{B}(\boldsymbol{X}) \cdot \boldsymbol{M}(x) - \boldsymbol{\xi}^{\mathrm{sv}}_{\mathrm{warping}}. \end{aligned}\right\} \tag{27}$$

From Fig. 5, it can be noted that the warpings associated to a traction T_x and those associated to bending moments M_y, M_z are significantly different for symmetric and antisymmetric cross-sections, whereas they are qualitatively similar for the other internal forces. The inverse situation is observed in the same Fig. 5 for the in plane deformations.

Fig. 6 is devoted to the well-known free edge effect detected in composite laminates under uniform axial extension (Pipes and Pagano, 1970; El Fatmi and Zenzri, 2002). For different values of θ, Fig. 6 presents the

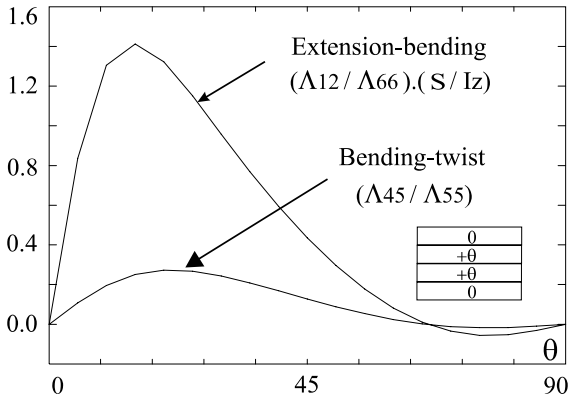

Fig. 2. Compliances associated to extension-bending and bending-twist couplings in symmetric laminated beams.

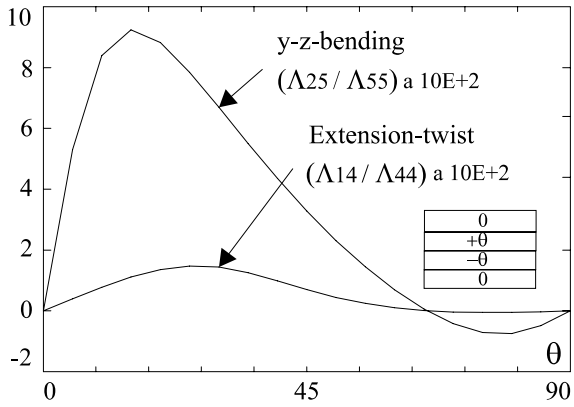

Fig. 3. Compliances associated to extension-twist and y–z-bending couplings in antisymmetric laminated beams.

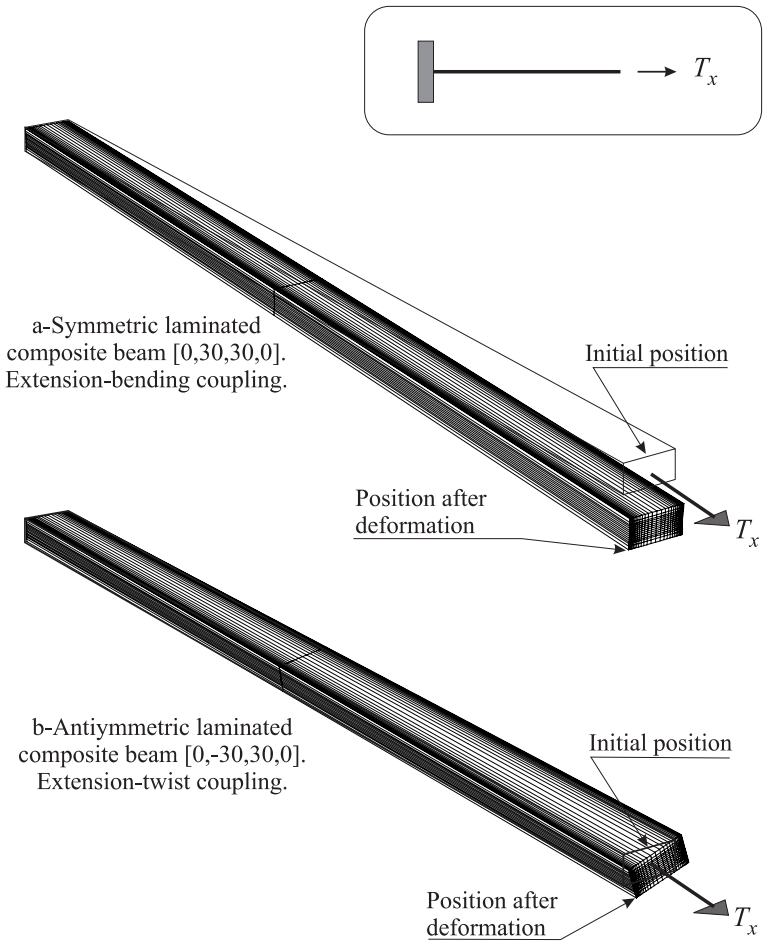

Fig. 4. Three-dimensional Saint–Venant deformation in laminated beams exhibiting elastic couplings in an extension test.

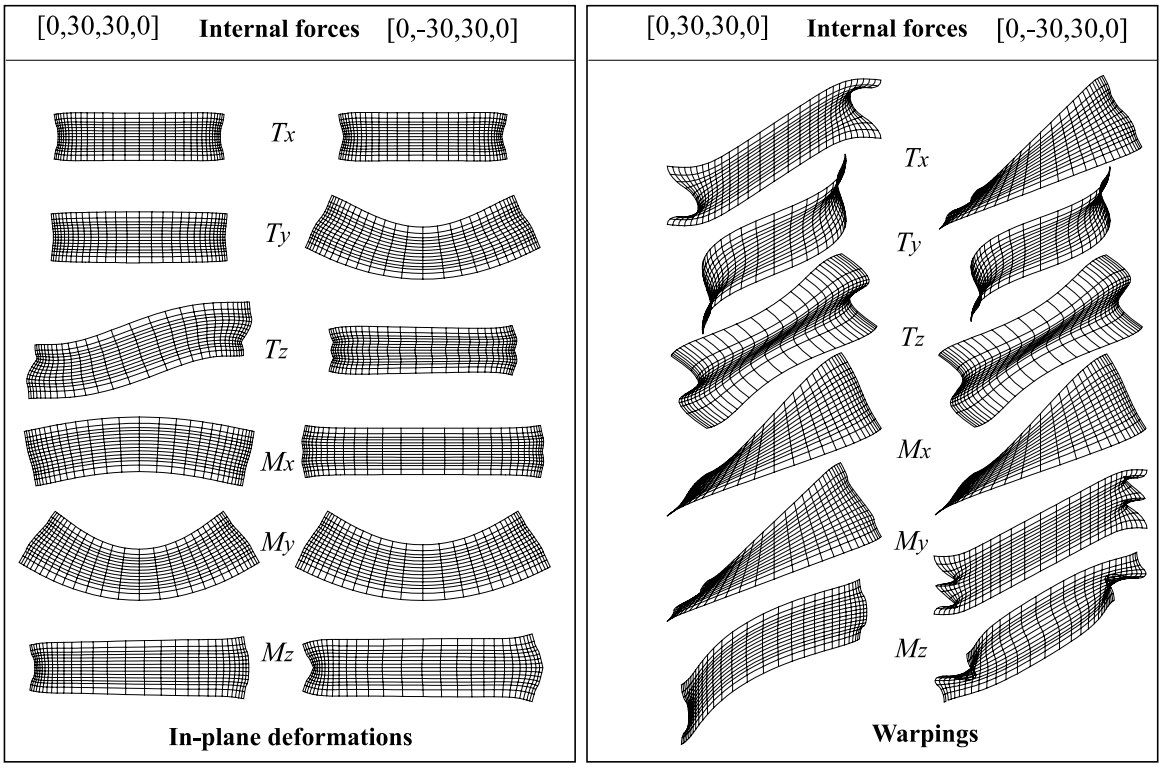

Fig. 5. Warpings and in-plane deformations associated to each of the internal forces in symmetric and antisymmetric laminated cross-sections.

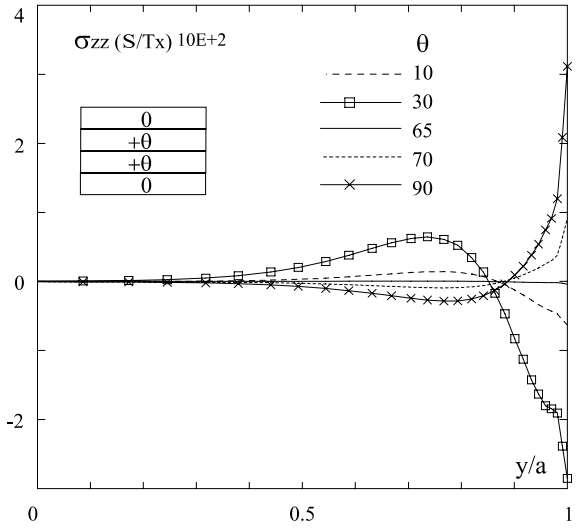

Fig. 6. Free edge effect in an extension test. Distribution of the interlaminar stress σ_{zz} along the interface $0 - \theta$.

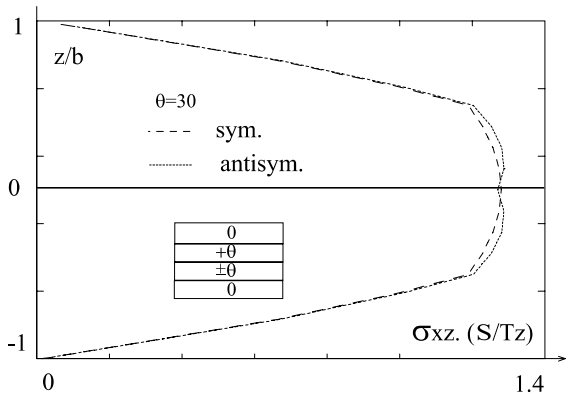

Fig. 7. Distributions of the shear stresses σ_{xz} within the thickness ($y = 0$) of symmetric and antisymmetric laminated cross-sections subjected to a shear force T_z.

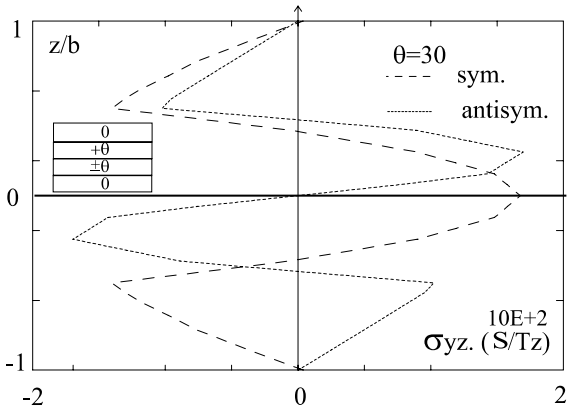

Fig. 8. Distributions of the shear stresses σ_{yz} within the thickness ($y = 0$) of symmetric and antisymmetric cross-sections subjected to a shear force T_z.

concentrations of the σ_{zz} stresses at the $0 - \theta$ interface and near the free edge, for beams subjected to a traction T_x; the results are nearly identical for symmetric and antisymmetric cross-sections. It appears that near the free edge the normal stresses σ_{zz} are of traction only when θ is greater than a value of about 65°. Finally, Figs. 7 and 8 present the variations within the cross-section thickness of the shear stresses σ_{xz} and σ_{yz} due to a shear force T_z.

6. Conclusion

The results presented in this paper on structural behavior and three-dimensional displacements and stresses for a representative set of sections, may be added to the first illustrations made by Sanchez (2001) and El Fatmi and Zenzri (2002) to show again the efficiency and accuracy of the exact beam theory in the study of arbitrary elastic multi-material cross-sections. The proposed numerical method uses three-dimensional available finite elements and classical elasticity formulation, which make it easy to implement

in standard elasticity softs. It constitutes an adequate tool for the study of the structural behavior of any cross-section and it provides three-dimensional Saint–Venant solutions which will allow the computations of local effects. This tool will also be useful for the analysis of experimental composite tests which are more structure tests rather than material tests.

Appendix A

This appendix is devoted to the relations, discussed in Section 4, that have to be imposed between the degrees of freedom of each finite element. These relations are here written for the reference finite elements of Fig. 9. In the following, $[u_i, v_i, w_i]$ denote the displacement components of the node i. The notations:

$$u = [u_1, u_2, \ldots, u_N], \quad v = [v_1, v_2, \ldots, v_N], \quad w = [w_1, w_2, \ldots, w_N], \quad \eta = [\eta_1, \eta_2, \ldots, \eta_N], \quad N = 15, 20,$$

are also used.

The 23 linear relations for the 15-node triangular prism element are as follows:

$$f_i(u) = 0; \quad i \in \{2, 5-9\},$$
$$f_i(v) = 0; \quad i \in \{1, 3, 5-9\},$$
$$f_i(w) = 0; \quad i \in \{1, 4, 5-9\},$$
$$f_4(v) + f_3(w) = 0,$$
$$f_3(u) + 2f_2(v) = 0,$$
$$f_4(u) + 2f_2(w) = 0,$$

where

$$f_1(\eta) = -\eta_1 + \eta_{10},$$
$$f_2(\eta) = \eta_{10} + \eta_1 - 2\eta_7,$$
$$f_3(\eta) = \eta_3 - 3\eta_{10} - \eta_{12} - 4\eta_2 + 3\eta_1 + 4\eta_{11},$$
$$f_4(\eta) = \eta_5 - 3\eta_{10} - 4\eta_6 + 3\eta_1 - \eta_{14} + 4\eta_{15},$$
$$f_5(\eta) = -4\eta_4 + 4\eta_6 + 4\eta_2 + 4\eta_{13} + 4\eta_{10} - 4\eta_{15} - 4\eta_{11} - 4\eta_1,$$
$$f_6(\eta) = \eta_3 - \eta_1 - \eta_{10} + \eta_{12} + 2\eta_7 - 2\eta_8,$$
$$f_7(\eta) = \eta_5 - \eta_1 - 2\eta_9 - \eta_{10} + 2\eta_7 + \eta_{14},$$
$$f_8(\eta) = -2\eta_3 - 2\eta_1 + 4\eta_2 + 2\eta_{12} + 2\eta_{10} - 4\eta_{11},$$
$$f_9(\eta) = -2\eta_5 - 2\eta_1 + 4\eta_6 - 4\eta_{15} + 2\eta_{10} + 2\eta_{14}.$$

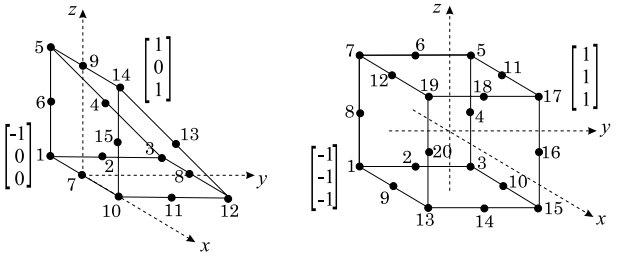

Fig. 9. The 15-node triangular prism element and the 20-node rectangular prism element in the reference system of coordinates.

The 32 linear relations for the 20-node rectangular prism element are as follows:

$$
\begin{aligned}
&g_i(u) = 0; \quad i \in \{2, 5-12\},\\
&g_i(v) = 0; \quad i \in \{1, 3, 5-12\},\\
&g_i(w) = 0; \quad i \in \{1, 4, 5-12\},\\
&g_4(v) + g_3(w) = 0,\\
&g_3(u) + 2g_2(v) = 0,\\
&g_4(u) + 2g_2(w) = 0,
\end{aligned}
$$

where

$$
\begin{aligned}
g_1(\eta) &= -2\eta_2 + 2\eta_{18} - \eta_{17} - 2\eta_6 + \eta_7 + 2\eta_{20} - 2\eta_4 + \eta_5 + 2\eta_{14} + \eta_3 - \eta_{15}\\
&\quad + \eta_1 + 2\eta_{16} - \eta_{13} - 2\eta_8 - \eta_{19},\\
g_2(\eta) &= \eta_7 + \eta_1 + \eta_{13} - 2\eta_{10} - 2\eta_{12} + \eta_3 + \eta_{17} + \eta_5 - 2\eta_9 - 2\eta_{11} + \eta_{19} + \eta_{15},\\
g_3(\eta) &= -2\eta_{20} - 2\eta_4 + 2\eta_{16} + 2\eta_8,\\
g_4(\eta) &= 2\eta_2 + 2\eta_{18} - 2\eta_{14} - 2\eta_6,\\
g_5(\eta) &= \eta_{17} + \eta_{13} - \eta_1 + \eta_3 + \eta_7 - \eta_5 - \eta_{15} - \eta_{19},\\
g_6(\eta) &= \eta_5 - \eta_{19} - 2\eta_{11} + \eta_{15} - \eta_7 - \eta_1 - \eta_{13} - 2\eta_{10} + 2\eta_{12} + \eta_3 + \eta_{17} + 2\eta_9,\\
g_7(\eta) &= \eta_{19} - \eta_{15} + \eta_7 - \eta_1 - \eta_{13} + 2\eta_{10} - 2\eta_{12} - \eta_3 + \eta_{17} + \eta_5 + 2\eta_9 - 2\eta_{11},\\
g_8(\eta) &= -\eta_3 + 2\eta_6 + 2\eta_2 + \eta_{19} - \eta_7 + \eta_{15} - 2\eta_{14} - \eta_5 + \eta_{13} - \eta_1 + \eta_{17} - 2\eta_{18},\\
g_9(\eta) &= -2\eta_{20} + \eta_{17} - \eta_5 - \eta_3 + 2\eta_4 - \eta_1 - \eta_7 + \eta_{13} + \eta_{15} + 2\eta_8 - 2\eta_{16} + \eta_{19},\\
g_{10}(\eta) &= \eta_{17} - 2\eta_9 + \eta_5 - \eta_{19} - 2\eta_{11} - \eta_{15} - \eta_7 + \eta_1 + \eta_{13} + 2\eta_{10} + 2\eta_{12} - \eta_3,\\
g_{11}(\eta) &= \eta_{17} - 2\eta_{18} + \eta_3 + 2\eta_6 - 2\eta_2 + \eta_{19} - \eta_7 - \eta_{15} + 2\eta_{14} - \eta_5 - \eta_{13} + \eta_1,\\
g_{12}(\eta) &= 2\eta_4 - \eta_{19} + \eta_{17} + 2\eta_{20} - \eta_3 - 2\eta_{16} - \eta_{13} + \eta_1 + \eta_{15} - 2\eta_8 + \eta_7 - \eta_5.
\end{aligned}
$$

References

Batoz, J.L., Dhatt, G., 1990. Modélisation des structures par éléments finis, vol. 1, Solides Elastiques. Hermès, Paris.

Debard, Y., 1997. Logiciel de calcul des structures par la méthode des éléments finis. Version RDM5.01. Institut Universitaire de Technologie, Le Mans, France.

El Fatmi, R., Zenzri, H., 2002. On the structural behaviour and the Saint–Venant solution in the exact beam theory. Application to laminated composite beam. Computers and structures 80 (16–17), 1441–1456.

Friedman, Z., Kosmatka, J.B., 2000. Torsion and flexure of a prismatic isotropic beam using the boundary element method. Computers and structures 74, 479–494.

Gay, D., 1998. Maréríaux composites. Hermes, France.

Karama, M., Afaq, K.S., Mistou, S., 2003. Mechanical behavior of laminated composite beam by the new multi-layered laminated composite structures model with transverse shear stress continuity. International Journal of Solids and Structures 40 (6), 1525–1546.

Kim, C., White, S.R., 1997. Thick-walled composite beam theory including 3-D elastic effects and torsional warping. International journal of solids and Structures 34 (31–32), 4237–4259.

Ladevèze, P., Simmonds, J.G., 1998. New concepts for linear beam theory with arbitrary geometry and loading. European Journal of Mechanics, A/Solids 17 (3), 377–402.

Ladevèze, P., Sanchez, P., Simmonds, J.G., 2001. On application of the exact theory of elastic beams. In: Durban, D., Givoli, D., Simmonds, J.G. (Eds.), Advances in the Mechanics of plates and Shells. Kluwer Academic Publishers.

Le Fichoux, E., 1998. Présentation et utilisation de CASTEM200. Rapport DMT/SEMT/LAMS/RT/98-014-A, CEA, France.

Pastor, J., 2000. Torsion des poutres hétérogènes: modélisation en contraintes et en déplacements. Revue Française de Génie Civil 4, 413–427.

Pipes, R.B., Pagano, N.J., 1970. Interlaminar stresses in composite laminates under uniform axial extension. Journal of Composite Materials 4, 538–548.

Rand, O., 2001. A multilevel analysis of solid laminated composite beams. International Journal of Solids and Structures 38 (22–23), 4017–4043.

Reddy, J.N., 1989. On refined computational models of composite laminates. International Journal for Numerical Methods in Engineering 27, 361–382.

Renton, J.D., 1991. Generalized beam theory applied to shear stiffness. International Journal of Solids and Structures 27 (15), 1955–1967.

Renton, J.D., 1997. A note on the form of the shear coefficient. International Journal of Solids and Structures 34 (26), 1681–1685.

Sanchez, P., 2001. Mise en oeuvre et illustration de la théhorie exacte des poutres. Thèse de Doctorat, E.N.S. Cachan, LMT 2001/2, France.

Soldatos, K.P., Watson, P., 1997. A general theory for the accurate stress analysis of homogeneous and laminated composite beams. International Journal of Solids and Structures 34 (22), 2857–2885.

Vlassov, B.Z., 1962. Pièces longues en voiles minces. Eyrolles, Paris.

Zienkiewicz, O.C., Zhu, J.Z., Cong, N.G., 1989. Effective and practical h–p adaptative analysis procedures for the finite element method. International Journal for Numerical Methods in Engineering 28, 879–891.